



Research article

Genome-wide transcriptional comparison of MPP⁺ treated human neuroblastoma cells with the state space model

Jin Hwan Do *

Department of Biomolecular and Chemical Engineering, DongYang University, Yeongju 750-711, South Korea

* **Correspondence:** Email jinhwando@dyu.ac.kr; Tel: +82-54-630-1361; Fax: +82-54-630-1275.

Abstract: This study compared a parkinsonian neurotoxin 1-methyl-4-phenylpyridinium (MPP⁺) response in two distinct phenotypes of human neuroblastoma cell lines: neuronal N-type SH-SY5Y cells and flat substrate-adherent S-type SH-EP cells. SH-SY5Y and SH-EP cells shared only 14% of their own MPP⁺ response genes, and their gene ontology (GO) analysis revealed significant endoplasmic reticulum (ER) stress by misfolded proteins. Gene modules, which are groups of transcriptionally co-expressed genes with similar biological functions, were identified for SH-SY5Y and SH-EP cells by using time-series microarray data with the state space model (SSM). All modules of SH-SY5Y and SH-EP cells showed strong positive auto-regulation that was often mediated via signal molecules and may cause bi-stability. Interactions in gene levels were calculated by using SSM parameters obtained in the process of module identification. Gene networks that were constructed from the gene interaction matrix showed different hub genes with high node degrees between SH-SY5Y and SH-EP cells. That is, key hub genes of SH-SY5Y cells were *DCN*, *HIST1H2BK*, and *C5orf40*, whereas those of SH-EP cells were *MSH6*, *RBCK1*, *MTHFD2*, *ZNF26*, *CTH*, and *CARS*. These results suggest that inhibition of the mitochondrial complex I by MPP⁺ might induce different downstream processes that are cell type dependent.

Keywords: neuroblastoma; 1-methyl-4-phenylpyridinium; cell death; Parkinson's disease; transcriptional regulation; gene networks; state space model

1. Introduction

Parkinson's disease (PD) is a common neurodegenerative disease that is characterized by the progressive loss of dopaminergic (DAergic) neurons in substantia nigra pars compacta (SNpc), which results in both motor and cognitive deficits with cardinal symptoms of bradykinesia, rigidity, tremor, and postural instability [1]. Many studies have been done to understand the pathogenesis of PD in experimental cell and animal models [2, 3]. However, its complete pathological mechanism remains unknown, thus making it difficult to develop efficient treatments to target the original cause of PD. It has been shown that people who are intoxicated with 1-methyl-4-phenyl-1, 2, 3, 6-tetrahydropyridine (MPTP) develop a syndrome that is nearly identical to PD [4]. Since this discovery, MPTP has become one of the most used neurotoxins that can induce PD-related DAergic neuronal death in mice and non-human primates. An active metabolite of MPTP, 1-Methyl-4-phenyl-pyridium (MPP⁺), is actively transported inside DAergic neurons by dopamine and noradrenaline transporters, resulting in the prevention of oxidative phosphorylation at the level of complex I and an increase in the steady state levels of mitochondrial superoxide [5].

Superoxide is the precursor of most reactive oxygen species (ROS) and a mediator in oxidative chain reactions. ROS lead to severe harmful effects to the cells when they are over-accumulated. This phenomenon is known as oxidative stress. Oxidative stress results in the generation and aggregation of misfolded proteins, which can also lead to excessive ROS and neurotoxicity [6]. In PD, the death of DAergic neurons can be caused by the over-accumulation and posttranslational modification of α -synuclein by oxidative stress [7, 8]. This indicates that oxidative stress might be one of the primary mechanisms behind the onset and progression of DAergic neurodegeneration [9]. Therefore, it is important to identify molecular key players, such as genes, proteins, and metabolites, in the downstream processes of oxidative stress for drug target discovery in PD.

A growing number of studies on postmortem PD samples suggest that the activation of common upstream components of PCD pathways may lead to the co-existence of different morphological types of cell death [10]. Co-existence of different morphological types of cell death suggests involvement of molecular pathways linked to PCD with diverse morphology of cell death [10]. Significant advances have been made in experimental studies of PD, especially through the use of pheochromocytoma (e.g., PC12) and human neuroblastoma (SH-SY5Y, SH-EP) cells. These cells mimic many aspects of the DAergic neuronal death that is observed in PD when treated with neurotoxins such as MPP⁺ and 6-hydroxydopamine (6-OHDA) [11]. Our previous work investigated genome-wide gene expression changes in two types of human neuroblastoma cells (SH-SY5Y [N-type] and SH-EP [S-type]) that were treated with MPP⁺ [12, 13]. Neuroblastoma cells have been grouped into three major types depending on morphologies and biochemical properties: neuroblastic (N-type) cells, substrate-adherent (S-type) cells and malignant neuroblastoma stem cells, called I-type (intermediate type) which expresses features of both N- and S-type cells [14]. Both SH-SY5Y and SH-EP cell lines were derivatives of the cell line, human neuroblastoma SK-N-SH.

In this study, parkinsonian neurotoxin MPP⁺ response genes and their interactions in MPP⁺-treated SH-SY5Y and SH-EP cells were compared with a linear Gaussian state space model (SSM) [15], which allows one to estimate an internal state vector representing the expression level of gene modules from time-series microarray data. Gene modules might represent groups of co-expressed genes that have similar biological functions from gene expression data of short time courses. There were only 14% common MPP⁺ response genes between N-type SH-SY5Y and S-type SH-EP cells, and gene networks that were estimated from time-series microarray data showed cell-type specificity. This indicates that

MPP⁺-induced neuronal cell death might be dependent on cell type. In addition, our results might be helpful for developing potential neuroprotective strategies for PD, as well as understanding the co-existence of apoptotic and nonapoptotic DAergic cell death in postmortem PD patients.

2. Materials and Method

2.1. Microarray data

Time-series microarray data were obtained from our previous reports [12, 13] and consisted of eight time points, including control (before MPP⁺ treatment) and 0.5, 1.5, 3, 6, 9, 12, and 24 h after MPP⁺ treatment for SH-SY5Y and SH-EP cells. Microarray data included three replicates and two replicates for each time point in SH-SY5Y and SH-EP cells, respectively. All microarray data were produced with the Illumina bead array (human HT-12 expression v.4 bead array), which includes the probes for 47,231 genes with well-established or provisional annotation. Raw expression data were log₂ transformed and normalized with quantile normalization. After the filtration of probe sets that were redundantly mapped to a single gene and probes that had no corresponding gene name, i.e., gene symbol, the remaining 32,421 probe sets all had one-to-one mapping to human gene symbols.

2.2. Identification of MPP⁺ response genes

Identification of the MPP⁺ response genes from time-series microarray data was carried out by a software package called EDGE [16]. To use this program, the relative expression level at each time point was required. Thus, the expression value of each time point was divided by that of control and was log₂ transformed. For example, let $z_i^{j,k}$ be the relative expression level (log₂ ratio) of gene i on replicate k , where there are $i = 1, 2, \dots, 32,421$ probe sets and $k = 1, 2, 3$ for SH-SY5Y cells and $k = 1, 2$ for SH-EP cells. For each replicate, there were $j = 1, \dots, 7$ time points (which correspond to 0.5, 1.5, 3, 6, 9, 12, 24 h after MPP⁺ treatment). The relative expression values are modeled by

$$z_i^{j,k} = \mu_i(t^{(j)}) + \xi_i^{j,k}$$

where $\mu_i(t^{(j)})$ is average (unknown) expression value for gene i evaluated at time $t^{(j)}$ and the average time curve $\mu_i(t)$ for gene i can be written in terms of a p -dimensional linear basis

$[s_1(t), \dots, s_p(t)]$:

$$\mu_i(t) = \beta_{0,i} + \beta_{i,1}s_1(t) + \beta_{i,2}s_2 + \dots + \beta_{i,p}s_p(t)$$

where $\beta_{0,i}$ is the intercept term, p is the same for all genes (the value of dimension p in this study was 3), and $\xi_i^{j,k}$ is the random deviation from this curve and is modeled as independent random variables

with mean zero and gene dependent σ_i^2 . To assess differentially expressed genes by MPP⁺ treatment, i.e., MPP⁺ response genes, the goodness-of-model fit under null hypothesis $H_{0,i}$ that $\mu_i(t) = 0$ was

compared to that under the alternative hypothesis $H_{1,i}$ formulated with the general parameterization

$\mu_i(t) = \beta_{0,i} + \beta_{i,1}s_1(t) + \beta_{i,2}s_2 + \beta_{i,3}s_3(t)$ with some non-zero coefficients, by calculating for gene i a F statistic similar to the one used in ANOVA:

$$F_i = \frac{SS_i^0 - SS_i^1}{SS_i^1}$$

where SS_i^0 is the sum of squares of the residuals obtained from the null model, and SS_i^1 is the sum of squares of the residuals obtained from the alternative model. The top 1,000 probes from the q -value rank were selected as MPP⁺ response genes, and the cut-off q -value was 0.01.

2.3. Gene Ontology (GO) analysis

For the estimation of GO terms that are significantly enriched in selected gene list, such as MPP⁺ response genes, a web-based program called *GOrilla* was employed [17]. This program uses hypergeometric distribution to identify significant GO terms. Given a total number of genes N with B of these genes associated with a particular GO term and n of these genes in the target set, the probability that b or more genes from the target set are associated with the given GO term is given by the hypergeometric tail:

$$\text{Pr ob}(X \geq b) = \sum_{i=b}^{\min(n,B)} \frac{\binom{n}{i} \binom{N-n}{B-i}}{\binom{N}{B}}$$

The *GOrilla* program has recognized 22,466 genes out of 31,421 gene symbols, and only 18,002 of these genes are associated with a GO term.

2.4. Identification of gene modules and module gene interactions with the SSM

To find gene modules from MPP⁺ response genes using time-series gene expression data, a linear Gaussian SSM proposed by Hirose et al. [15] was employed. In the SSM, state variables are used to represent unobservable biological entities, such as transcription factors or protein complexes, and temporal gene expression profiles are mapped to the state variables to model the dynamics and dependencies of the state variables. Briefly, let $y_t \in R^p$, $t \in T_{obs} \subseteq T$ be a series of vectors containing observed expression levels of p genes at the t -th time points. In this study, the value of p and t was 1,000 and 8, respectively. A sequence of the observation vectors, $Y_{T_{obs}} = \{y_t\}$, $n \in T_{obs}$, is modeled by supposing that y_t is generated from the k -dimensional hidden-state variable denoted by x_t . In this study, the dimension of state variable was chosen as four (i.e., $k = 4$), based on the BIC suggested by Yamaguchi et al. [18], for the SSM of SH-SY5Y and SH-EP cells. The SSM is shown as follows.

$$\begin{aligned} x_t &= Fx_{t-1} + v_t, \quad t \in T \quad (\text{system model}) \\ y_t &= Hx_t + w_t, \quad t \in T_{obs} \quad (\text{observation model}) \end{aligned}$$

where F is the state transition matrix ($k \times k$), H is the observation matrix ($p \times k$), and $v_t \sim N_k(0_k, Q)$ and $w_t \sim N_p(0_p, R)$ ($v_t \sim N_k(0_k, Q)$ and $w_t \sim N_p(0_p, R)$) are the system noise and the observation noise, respectively. The initial state vector x_0 is assumed to be a Gaussian random vector with mean vector μ_0 and covariance matrix Σ_0 , i.e., $x_0 \sim N_k(\mu_0, \Sigma_0)$. Parameters including H, F, R, Q, μ_0 , and the state vector in the model were estimated using the SiGN-SSM software [19] under the following constraints:

- $Q = I_k$
- $H^T R^{-1} H = \Lambda \equiv \text{diag}(\lambda_1, \dots, \lambda_k)$ where $\lambda_1 > \lambda_2 > \dots > \lambda_k$
- An arbitrary sign condition is imposed on the elements of the first row of H

After the estimation of parameters, gene expression vectors (y_t) can be mapped onto the state space R^k with the projection matrix D ($k \times p$) as follows:

$$x_t = DR^{-1/2}(y_t - w_t), \quad t \in T_{obs}$$

$$D = \Lambda^{-1} H^T R^{-1/2}$$

The gene module is identified by using the above projection matrix. That is, the element in the i -th row and j -th column of projection matrix D ($k \times k$) represents the effects of the j -th gene on the i -th module and was designated as d_{ij} . If genes have large $|d_{ij}|$ for each module (each row of matrix D), then groups of genes, i.e., modules, can be obtained. In this study, four gene modules including 100 genes were obtained by selection of the highest and lowest ranked 50 genes in each row of projection matrix D . As the signs of d_{ij} , which corresponds to the highest and lowest ranked 50 genes in each row of projection matrix D , were positive and negative, respectively, each module could also be divided into two sub-modules (i.e., M_{i+} and M_{i-}).

The interactions or regulation structures at gene levels were obtained by the conversion of the SSM into a parsimonious representation of the first-order vector autoregressive form, as shown below:

$$R^{-1/2}(y_n - w_n) = \Psi R^{-1/2}(y_{n-1} - w_{n-1}) + R^{-1/2} H v_n$$

where the autoregressive coefficient matrix is given by $\Psi \equiv D^T \Lambda F D$. Matrix Ψ ($p \times p$) represents temporal interactions in gene level in the following manner: once the k modules $x_{n-1} = DR^{-1/2}(y_{n-1} - w_{n-1})$ are given at time $n-1$, the current module are calculated with the scaled-system matrix ΛF as $\Lambda F x_{n-1} = \Lambda F D R^{-1/2}(y_{n-1} - w_{n-1})$.

2.5. Construction of gene regulation networks and visualization

The Interaction matrix Ψ_m between module genes was obtained by extraction of the elements corresponding to module genes in the matrix Ψ estimated in the SSM. As the total number of module genes was 331 in SH-SY5Y and 318 in SH-EP cells, the size of Ψ_m was 331×331 and 318×318 for SH-SY5Y and SH-EP cells, respectively. Gene networks were constructed by the selection of elements satisfying $|\Psi_{m,ij}| > 0.012$, where the edge density was nearly constant for both cases of SH-SY5Y and SH-EP cells. The estimated networks were visualized by using Cytoscape v3.2.1 (<http://www.cytoscape.org>), and communities inside the networks were determined with Cytoscape plug-in ModuLand [20].

3. Results and Discussion

3.1. Comparison of MPP⁺ response genes between SH-SY5Y and SH-EP cells

Time-series microarray data for MPP⁺-treated neuroblastoma SH-SY5Y and SH-EP cells were obtained from previous studies [12, 13]. These microarray data consisted of control (time 0) and seven time points (0.5, 1.5, 3, 6, 9, 12, and 24 h) after MPP⁺ treatment, and each time point was repeated three times for SH-SY5Y cells and two times for SH-EP cells. Prior to the comparison of SH-SY5Y and SH-EP cells, differentially expressed genes (DEGs) during the time course were identified with the Extraction of Differential Gene Expression (EDGE) program [16], which introduces the time variable through a gene expression curve expanded over the polynomial or B-spline basis with the coefficients. The most significant curves were selected by q -values using a false discovery ratio (FDR)-like procedure. From the rank by q -value, the top thousands of genes were selected from 32,421 genes for both types of cells. These selected genes were considered to be MPP⁺ response genes, and the q -value cutoff was 0.01. The number of common MPP⁺ response genes between SH-SY5Y and SH-EP cells was 140, and the remaining 1,720 genes were cell type specific. This indicates that the molecular response of MPP⁺ toxicity might differ between SH-SY5Y and SH-EP cells. On the other hand, common MPP⁺ response genes between SH-SY5Y and SH-EP cells might be involved in core mechanisms for MPP⁺ toxicity.

To examine gene ontology (GO) terms that are significantly overrepresented in the 140 MPP⁺ response genes between SH-SY5Y and SH-EP cells, the web-based program *GOrilla* [17] was employed. The results are shown in Table 1. Most of the significantly enriched GO biological process (BP) terms showed involvement in the positive regulation of transcription in response to endoplasmic reticulum (ER) stress. This indicates that ER stress might play a key role in MPP⁺-induced neuronal cell death. In addition, the significant enrichment of CHOP (CCAAT/enhancer-binding protein)-ATF4 (activating transcription factor 4) complex in GO cellular component (CC) terms suggests that the expression of CHOP-ATF4-targeted genes might be changed by MPP⁺ treatment.

Most of the common MPP⁺ response genes showed similar expression patterns. However, the gene expression of 13 common MPP⁺ response genes represented clear contrasts at 12 and 24 h after MPP⁺ treatment (Table 2). Genes such as *ETS2*, *ZHX2*, *H1F0*, *C10orf35*, and *CNBP* showed down-regulation and up-regulation in SH-SY5Y and SH-EP cells, respectively. In contrast, the opposite regulation in both types of cells was observed for *CTDSPL*, *ABCB6*, *DACT3*, *P704P*, *TMBIM4*, and

ODZ4. In SH-SY5Y cells, down-regulation of *HIF1* might induce defects in nucleosome structure, whereas up-regulation of *TMBIM4* may inhibit MPP⁺ toxicity-induced apoptosis. In SH-EP cells, down-regulation of *ABCB6* may decrease the adenosine triphosphate-dependent uptake of toxic molecules, such as MPP⁺, into mitochondria, whereas up-regulation of transcription factors, such as *ETS2*, *ZHX2*, and *CNBP*, might contribute to changes in the expression of other MPP⁺ response genes. The existence of the differential regulation of common MPP⁺ response genes indicates that cellular downstream mechanisms toward the same neurotoxin (i.e., MPP⁺) might be cell type dependent. Both SH-SY5Y and SH-EP cells are derived via sub-cloning of SK-N-SH cells, but they are morphologically different. SH-SY5Y is an N-type cell line that expresses neurotransmitters and various neuronal cell-surface markers, whereas SH-EP is an epithelial substrate-adherent Schwannian (S-type) cell line that expresses proteins that are characteristic of Schwann cells and lack neuronal markers [14]. The physiological and genomic differences between these two types of cells might be responsible for the differential regulation of the same genes toward MPP⁺ toxicity.

Table 1. Gene Ontology (GO) analysis for 140 common MPP⁺ response genes between SH-SY5Y and SH-EP cells.

	GO Term	Description	<i>p</i> -value
BP	GO:0006520	cellular amino acid metabolic process	2.15E-05
	GO:0036499	PERK-mediated unfolded protein response	6.58E-05
	GO:1990440	positive regulation of transcription from RNA polymerase II promoter in response to endoplasmic reticulum stress	6.58E-05
	GO:0043038	amino acid activation	3.49E-04
	GO:0043039	tRNA aminoacylation	3.49E-04
	GO:0036003	positive regulation of transcription from RNA polymerase II promoter in response to stress	4.38E-04
	GO:0042026	protein refolding	4.38E-04
	GO:0009991	response to extracellular stimulus	4.57E-04
	GO:0061001	regulation of dendritic spine morphogenesis	5.70E-04
MF	GO:0035312	5'-3' exodeoxyribonuclease activity	2.76E-04
CC	GO:0036488	CHOP-C/EBP complex	4.65E-05
	GO:1990617	CHOP-ATF4 complex	4.65E-05
	GO:0044424	intracellular part	4.04E-04

BP: biological process, MF: molecular function, CC: Cellular component

Table 2. Thirteen MPP⁺ response genes showing different regulation between SH-SY5Y and SH-EP cells and their fold changes at 12 and 24 h after MPP⁺ treatment.

Gene	Definition	SH-SY5Y cells		SH-EP cells	
		12 h	24 h	12 h	24 h
ETS2	v-ets erythroblastosis virus E26 oncogene homolog 2 (avian) (ETS2), mRNA.	0.65	0.68	2.23	2.20
ZHX2	zinc fingers and homeoboxes 2 (ZHX2), mRNA.	0.79	0.95	1.16	2.50
FLJ35024	hypothetical LOC401491 (FLJ35024), non-coding RNA.	0.71	0.95	1.35	1.96
H1F0	H1 histone family, member 0 (H1F0), mRNA.	0.62	0.91	1.30	1.22
CTDSPL	CTD (carboxy-terminal domain, RNA polymerase II, polypeptide A) small phosphatase-like (CTDSPL), transcript variant 2, mRNA.	1.31	1.17	0.69	0.46
ABCB6	ATP-binding cassette, sub-family B (MDR/TAP), member 6 (ABCB6), nuclear gene encoding mitochondrial protein, mRNA.	1.06	1.24	0.62	0.63
DACT3	dapper, antagonist of beta-catenin, homolog 3 (<i>Xenopus laevis</i>) (DACT3), mRNA.	1.17	1.06	0.49	0.45
P704P	PREDICTED: prostate-specific P704P (P704P), mRNA.	1.14	1.04	0.85	0.51
FCGBP	Fc fragment of IgG binding protein (FCGBP), mRNA.	0.87	0.97	1.02	1.23
TMBIM4	transmembrane BAX inhibitor motif containing 4 (TMBIM4), mRNA.	1.14	1.04	0.83	0.65
ODZ4	odz, odd Oz/ten-m homolog 4 (<i>Drosophila</i>) (ODZ4), mRNA.	1.08	1.11	0.33	0.13
C10orf35	chromosome 10 open reading frame 35 (C10orf35), mRNA.	0.76	0.82	1.51	2.15
CNBP	CCHC-type zinc finger, nucleic acid binding protein (CNBP), transcript variant 3, mRNA.	0.90	0.89	1.40	1.80

3.2. Identification of gene modules in MPP⁺-treated SH-SY5Y and SH-EP cells with SSM

Modularity is recognized as a design principle in biological systems, as it has been observed in protein-protein interactions, metabolic networks, and transcriptional regulation networks [21]. The identification of gene modules involved in MPP⁺-induced neuronal cell death might open a way to systems approach to PD. Here, the time-series microarray data of MPP⁺-treated SH-SY5Y and SH-EP cells were used to find gene modules, which represent groups of transcriptionally co-expressed genes with similar biological functions. In this study, a linear Gaussian SSM, which was suggested by Hirose et al. [15], was employed for the identification of gene modules using time-dependent gene expression values of MPP⁺ response genes in SH-SY5Y and SH-EP cells. In the SSM, a gene module is considered as a set of genes that are regulated in concert by a shared program that governs their behavior [15]. To find gene modules for MPP⁺-treated SH-SY5Y and SH-EP cells, a sequence of 1,000-dimensional observation vectors $\{y_1, y_2, \dots, y_8\}$ (i.e., gene expression values at 8 time points for 1,000 MPP⁺

response genes) was modeled by assuming that at each time step, y_t was generated from a k -dimensional hidden-state variable that was denoted by x_t . Furthermore, the sequence $\{x_1, x_2, \dots, x_8\}$ defined a first-order Markov process. The dimension of state vector k was determined was chosen by minimizing Bayesian information criterion (BIC). Here, $k = 4$ was used for SH-SY5Y and SH-EP cells. The SSM can be described by the two following equations:

$$\begin{aligned}x_t &= Fx_{t-1} + v_t, \quad t \in \{1, 2, \dots, 8\} \quad (\text{system model}) \\y_t &= Hx_t + w_t, \quad t \in \{1, 2, \dots, 8\} \quad (\text{observation model})\end{aligned}$$

where F is the state transition matrix (4×4), H is the observation matrix (1000×4), $v_t \sim N_4(0_4, Q)$ is the system noise, and $w_t \sim N_{1000}(0_{1000}, R)$ is the observation noise. The initial state vector x_0 is assumed to be a Gaussian random vector with mean vector μ_0 and covariance matrix Σ_0 , i.e., $x_0 \sim N_k(\mu_0, \Sigma_0)$. Parameters, including H, F, R, Q, μ_0 , and the state vector x_t , were estimated using maximum likelihood estimation with the EM algorithm [15, 19]. As the number of time points was too small compared with that of MPP⁺ response genes, all replicates of time-series expression data were incorporated into the parameter estimation. All the parameters in the SSM were estimated with the SiGN-SMM software [19], which estimates a SSM for analyzing short-time and/or replicated time-series gene expression profiles.

During the parameter estimation process, the state vectors were constructed such that they were likely to follow the first-order Markov process:

$$x_t = DR^{-1/2}(y_t - w_t), \quad t \in \{1, 2, \dots, 8\}$$

where D is the projection matrix (4×1000) and defined by $(H'R^{-1}H)^{-1}H'R^{-1/2}$. The element in the i -th row and j -th column of matrix D represents effects of the j -th gene on the i -th module and was designated as d_{ij} . Gene modules, which are relevant to temporal gene expression patterns, were identified by selecting genes that have large $|d_{ij}|$ in each row of matrix D . That is, the genes at each module were selected according to the following method: the j -th gene was associated to the i -th positive module M_{i+} or the i -th negative module M_{i-} if the element d_{ij} in the i -th row of matrix D was ranked in the highest or lowest 50, respectively. As the number of rows in matrix D is "4", 4 modules were identified, and each module included 2 sub-modules. The expression profiles of module genes in SH-SY5Y and SH-EP cells are shown in Figure 1.

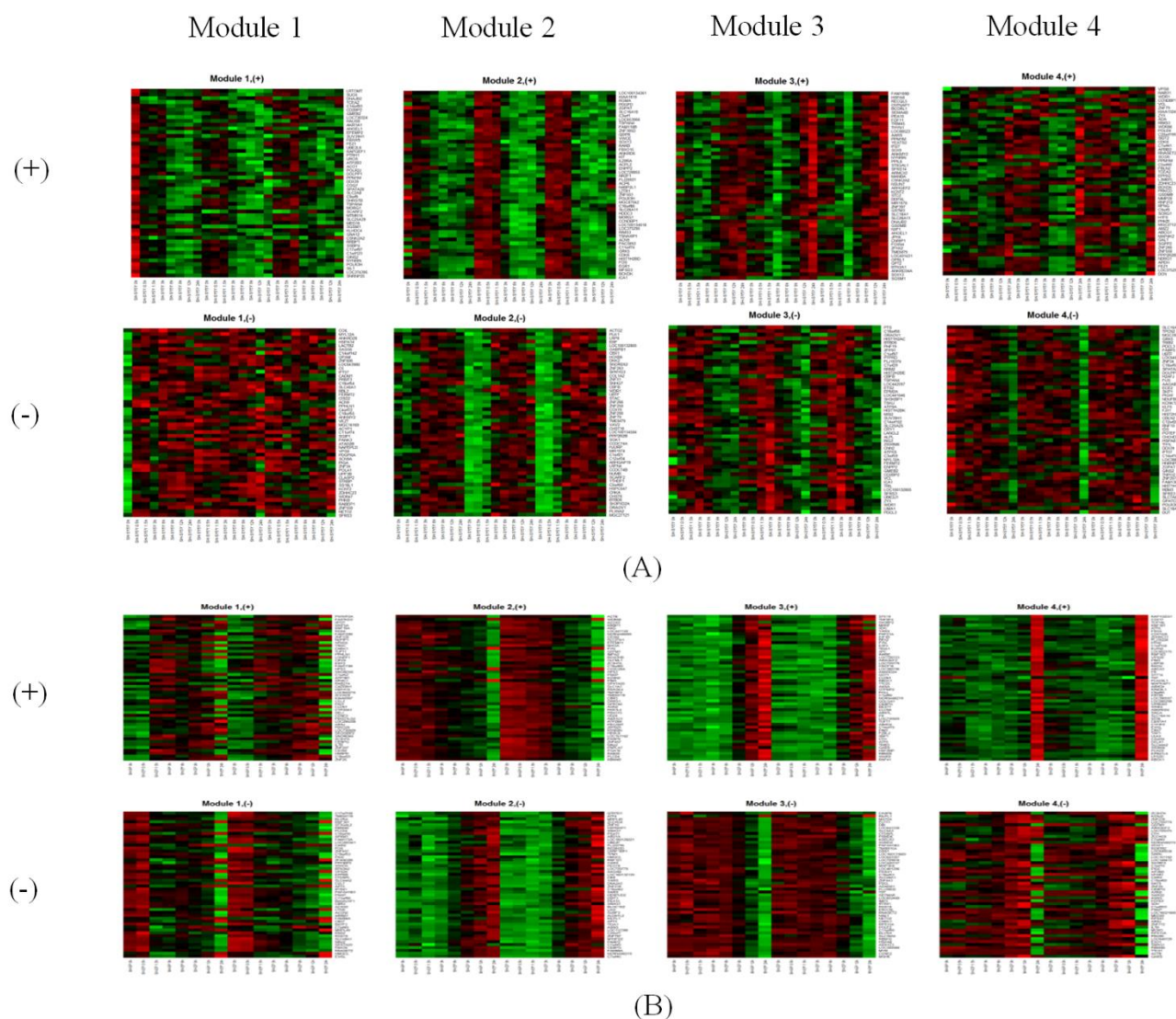


Figure 1. Heat-maps of temporal gene expression values. Row and column of each gene module represent gene and time, respectively. The column is listed in time order in each replicate, which consists of eight time points (0, 0.5, 1.5, 3, 6, 9, 12, and 24h). Green indicates low expression while red indicates high expression. (A) SH-SY5Y cells with three replicates. (B) SH-EP cells with two replicates.

The genes located at the same sub-modules represented very similar expression patterns as well as good reproducibility for replicates. The aggregation of genes with similar expression patterns indicates the high relevance of the genes in each module. Table 3 shows over-represented GO BP terms in each module of SH-SY5Y and SH-EP cells. The relevance of module genes for the GO BP was more apparent in SH-EP cells than in SH-SY5Y cells. For example, in SH-EP cells, the genes in M_{1+} represented enrichment of GO terms related to nucleic acid transport, whereas those in M_{3-} showed over-representation of GO terms related to cell cycle. This indicates that genes belonging to the same module might be involved in similar biological processes. Also, each module might play a role in the cellular response to MPP⁺ treatment. Table S1 shows gene information for each module.

Table 3. GO analysis for each module in SH-SY5Y and SH-EP cells.

Cell type	Module	GO Term	Description	<i>p</i> -value
SH-SY5Y	M ₁₊	–		
	M ₁₋	–		
	M ₂₊	GO:0002068	glandular epithelial cell development	4.31E-04
		GO:0050730	regulation of peptidyl-tyrosine phosphorylation	9.52E-04
	M ₂₋	–		
	M ₃₊	GO:0050885	neuromuscular process controlling balance	2.48E-04
		GO:0022404	molting cycle process	7.41E-04
		GO:0022405	hair cycle process	7.41E-04
	M ₃₋	GO:0042754	negative regulation of circadian rhythm	4.48E-04
	M ₄₊	GO:0003323	type B pancreatic cell development	2.84E-04
		GO:0002068	glandular epithelial cell development	5.70E-04
	M ₄₋	GO:0000377	RNA splicing, via transesterification reactions with bulged adenosine as nucleophile	1.11E-04
		GO:0000398	mRNA splicing, via spliceosome	1.11E-04
		GO:0000375	RNA splicing, via transesterification reactions	1.26E-04
	SH-EP	M ₁₊	GO:0006405	RNA export from nucleus
GO:0050657			nucleic acid transport	4.33E-04
GO:0051236			establishment of RNA localization	4.33E-04
GO:0015931			nucleobase-containing compound transport	9.17E-04
M ₁₋		GO:0098506	polynucleotide 3' dephosphorylation	6.39E-06
		GO:0098501	polynucleotide dephosphorylation	3.82E-05
		GO:0051187	cofactor catabolic process	8.48E-04
M ₂₊		GO:1901617	organic hydroxy compound biosynthetic process	7.30E-05
		GO:0046165	alcohol biosynthetic process	1.65E-04
		GO:0044282	small molecule catabolic process	4.60E-04
		GO:1901616	organic hydroxy compound catabolic process	6.11E-04
M ₂₋		GO:0006520	cellular amino acid metabolic process	1.82E-09
		GO:0019752	carboxylic acid metabolic process	8.02E-07
		GO:0036499	PERK-mediated unfolded protein response	2.04E-06
		GO:0006984	ER-nucleus signaling pathway	4.05E-05
		GO:0030968	endoplasmic reticulum unfolded protein response	6.61E-05
		GO:0006418	tRNA aminoacylation for protein translation	1.25E-04
		GO:0042219	cellular modified amino acid catabolic process	5.39E-04
GO:0009991	response to extracellular stimulus	7.32E-04		

M ₃₊	GO:1901653	cellular response to peptide	3.28E-05
	GO:0006990	positive regulation of transcription from RNA polymerase II promoter involved in unfolded protein response	3.33E-05
	GO:0006418	tRNA aminoacylation for protein translation	1.68E-04
	GO:0036500	ATF6-mediated unfolded protein response	1.99E-04
	GO:0060546	negative regulation of necroptotic process	1.99E-04
	GO:0032755	positive regulation of interleukin-6 production	3.40E-04
	GO:0034976	response to endoplasmic reticulum stress	7.27E-04
M ₃₋	GO:1903047	mitotic cell cycle process	1.36E-05
	GO:0010948	negative regulation of cell cycle process	1.00E-04
	GO:1901991	negative regulation of mitotic cell cycle phase transition	2.53E-04
	GO:0044772	mitotic cell cycle phase transition	3.07E-04
	GO:1901988	negative regulation of cell cycle phase transition	3.28E-04
M ₄₊	GO:0019869	chloride channel inhibitor activity	1.99E-04
	GO:0017081	chloride channel regulator activity	4.98E-04
M ₄₋	GO:0006418	tRNA aminoacylation for protein translation	1.16E-04
	GO:0006807	nitrogen compound metabolic process	1.20E-04
	GO:0006725	cellular aromatic compound metabolic process	5.70E-04
	GO:0090304	nucleic acid metabolic process	8.81E-04

The estimated matrix $F (4 \times 4)$ included the temporal relationship between modules, as shown in the system model. That is, the element in the i -th row and j -th column of matrix F represented the effects of the j -th module on the i -th module. These interactions between modules are shown in Figure 2. In both SH-SY5Y and SH-EP cells, all modules showed a self-loop edge with positive regulation, and their strengths were stronger than those among other modules. Positive auto-regulation in gene regulation networks is often mediated through signal molecules and may cause bi-stability [22]. Thus, the positive auto-regulation of modules that include cellular damage-related genes might result in cell death. Weak regulation among modules indicates that genes in each module might be barely affected by genes that belong to the other module. On the other hand, strong self-regulation of each module suggests that genes in each module might be highly associated.

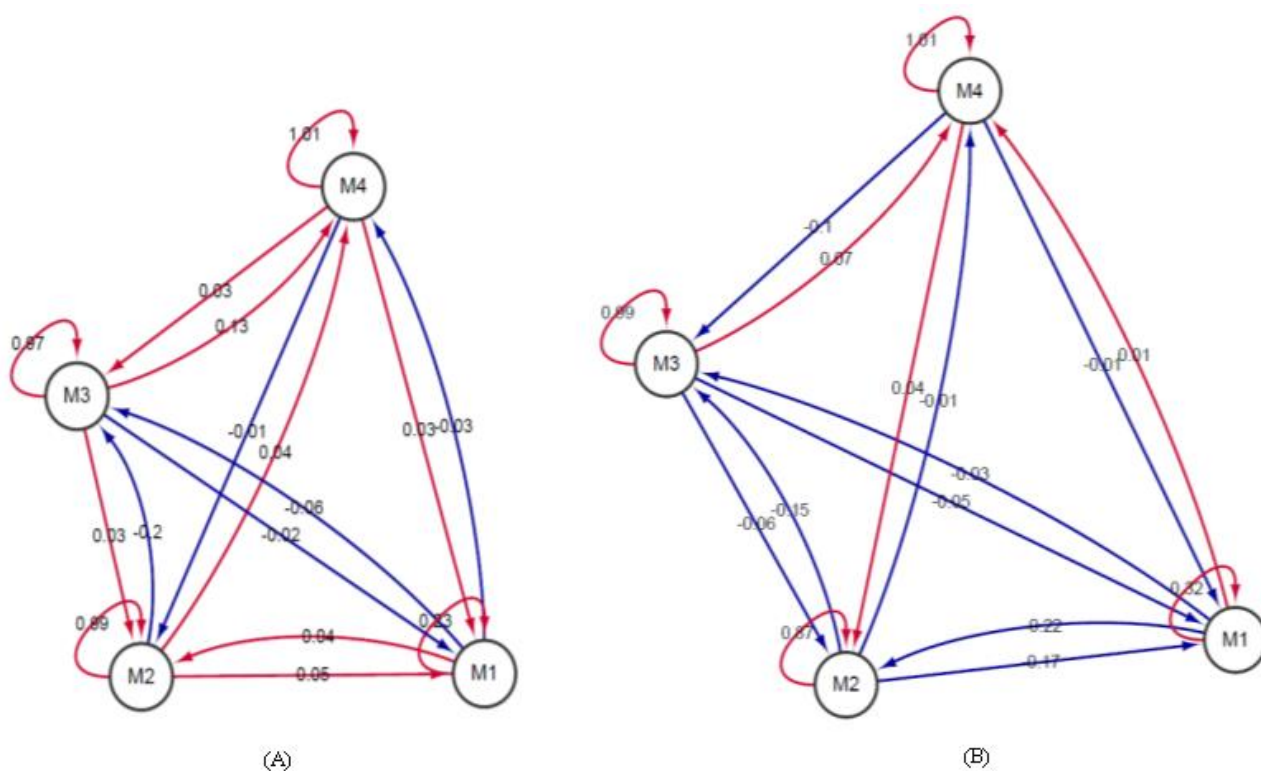


Figure 2. Estimation of module interactions by the SSM with time-series microarray data. (A) SH-SY5Y cells. (B) SH-EP cells. The positive and negative associations are represented by red and blue arrows, respectively.

3.3. Estimation of module genes' regulation structure in MPP^+ -treated SH-SH5Y and SH-EP cells from the SSM

The SSM that was employed for the estimation of gene modules can be converted to the first-order autoregressive form [15], as shown below:

$$R^{-1/2}(y_t - w_t) = \Psi R^{-1/2}(y_{t-1} - w_{t-1}) + R^{-1/2}H_t v_t$$

$$\Psi = D^T \Lambda F D, \Lambda = H^T R^{-1} H$$

where all parameter matrixes, including $R(p \times p)$, $D(k \times p)$, $\Lambda(k \times k)$, $F(k \times k)$, and $H(p \times k)$ (here, p —the number of MPP^+ response genes, and k —dimension of state variable, are 1000 and 4, respectively), have already been calculated during the gene module estimation process with the SSM in the previous section. The coefficient matrix $\Psi(1000 \times 1000)$ represents the temporal structure of gene-level networks in the following way: once the k modules $x_{t-1} = DR^{-1/2}(y_{t-1} - w_{t-1})$ are given at time $t-1$, the current modules are generated with the scaled-system matrix ΛF as $\Lambda F x_{t-1} = \Lambda F DR^{-1/2}(y_{t-1} - w_{t-1})$. In addition, the current modules regulate expression values of p genes in y_t with the reconstruction matrix D^T as $D^T \Lambda F x_{t-1} = \Psi R^{-1/2}$. Thus, matrix D , F and Ψ in the SSM correspond to transcriptional

modulation, module-module interactions, and gene-gene interactions, respectively. The element in the i -th row and j -th column of matrix Ψ represents the effects of the j -th gene on the i -th gene and was designated as Ψ_{ij} . The absolute value of Ψ_{ij} represents the regulation strength, and the sign of Ψ_{ij} indicates activation (+, positive regulation) or inhibition (−, negative regulation). The regulation structure between module genes might be important for understanding the underlying cellular mechanism of MPP⁺-induced neuronal cell death. Thus, instead of all MPP⁺ response genes, we focused on interactions between module genes that were identified in the previous section. In SH-SY5Y and SH-EP cells, the total number of modules was 4, and each module included 100 MPP⁺ response genes. However, the total number of module genes was 331 and 318 in SH-SY5Y and SH-EP cells, respectively. This was due to the existence of genes belonging to multiple modules. To investigate interactions between module genes, the module gene interaction matrix Ψ_m was constructed by selection of Ψ_{ij} corresponding to module genes.

Thus, the size of Ψ_m was 331×331 and 318×318 for SH-SY5Y and SH-EP cells, respectively. The topology of gene interaction or regulation network is generally sparse, i.e., a small constant number of edges per node, much smaller than the total number of nodes. To construct sparse networks from the module gene interaction matrix Ψ_m , a threshold for interaction value can be used. Because an almost constant average edge density of estimated networks from the module gene interaction matrix Ψ_m was observed at near a threshold of 0.012 for both SH-SY5Y and SH-EP cells, 0.012 was used as the threshold. That is, the only elements satisfying $|\Psi_m| > 0.012$ were selected for the construction of the sparse gene network. Estimated gene networks with a threshold of 0.012 for SH-SY5Y cells included 249 edges and 87 nodes, and had an average edge density of 2.86 (Figure 3). The color of edge in the figure represents regulation type (i.e., red for activation and blue for inhibition), and its width indicates regulation strength. Three communities were identified with Cytoscape plug-in ModuLand [20] from the networks of SH-SY5Y cells, and the nodes (genes) in the same community are shown with the same color. Genes including *DCN* (decorin) and *HIST1H2BK* (histone cluster 1) showed high node degrees in the leftmost community, whereas *C5orf40* (fibronectin type III domain containing 9) and *SGSM1* (small G protein signaling modulator 1) represented high node degrees in the middle and rightmost community, respectively (Figure 3). The relationship of hub genes, such as *DCN*, *HIST1H2BK*, and *C5orf40*, to the cellular structure indicates that MPP⁺ toxicity in SH-SY5Y cells might induce instability of the cellular structure.

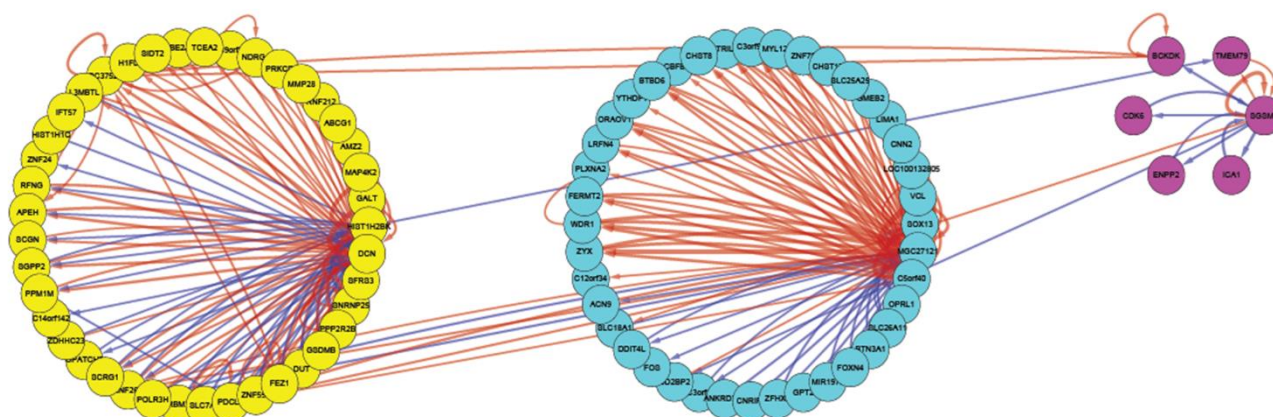


Figure 3. Estimated gene networks with a threshold of 0.012 for SH-SY5Y cells. The positive and negative associations are represented by red and blue arrows, respectively. The networks consisted of three communities and each community was gathered with same color of node.

The regulation structure between genes with node degrees above four is shown in Figure 4. Strong positive auto-regulation was observed at hub genes, such as *DCN*, *HIST1H2BK*, and *C5orf40*. A zinc finger protein 266 (*ZNF266*) showed positive association with two hub genes, including *DCN* and *MGC27121*, but showed negative association with *HIST1H2BK*. *ZNF266* was located in a cluster of similar genes encoding zinc finger proteins on chromosome 19 and may be involved in gene regulation. At 24 h after MPP⁺ treatment, *DCN* was upregulated (fold change = 2.4), whereas *HIST1H2BK* was down-regulated (fold change = 0.30). These regulation patterns showed a good agreement with estimated regulation structure between these genes. *SGSM1* showed no association with other genes, as none of the genes that were directly connected to *SGSM1* had more than four edges. In the community with purple nodes (Figure 3), all genes except for *TMEM79* (transmembrane protein 79) showed negative association with *SGSM1*. This regulation structure showed a good agreement with the time-dependent expression patterns of genes in the community (Table S2). That is, the expression values of *TMEM79* and *SGSM1* showed time-dependent increases, whereas those of *BCKDK* (branched chain ketoacid dehydrogenase), *CDK6* (cyclin dependent kinase 6), *ENPP2* (ectonucleotide pyrophosphatase/phosphodiesterase 2), and *ICA1* (islet cell autoantigen 1) represented time-dependent decrease. *BCKDK* is found in the mitochondrion, where it phosphorylates and inactivates BCKD. Thus, down-regulation of *BCKDK* might be related to mitochondrial stress.

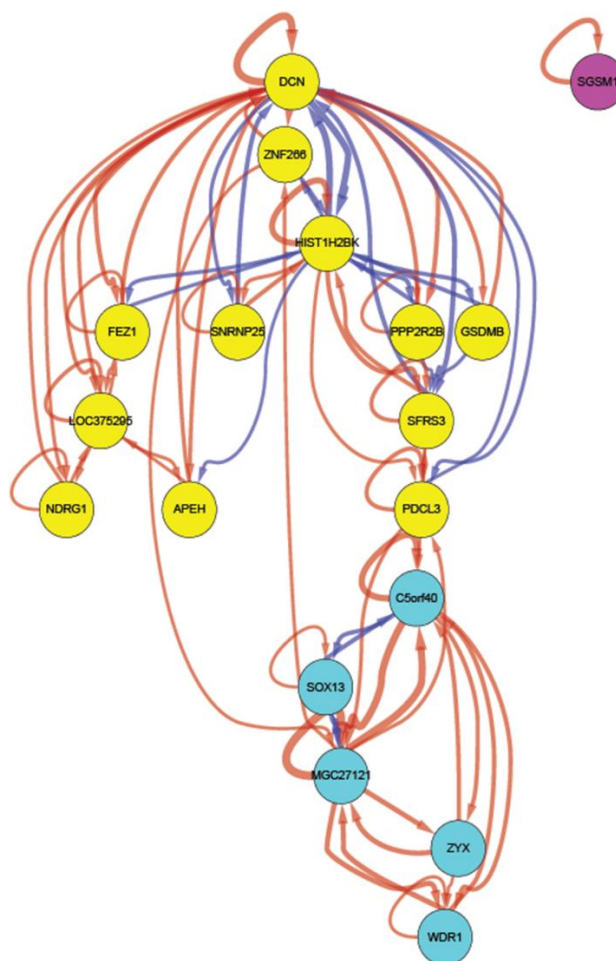


Figure 4. Sub-networks extracted from Figure 3 by selection of nodes, which have node degrees above 4. The positive and negative associations are represented by red and blue arrows, respectively. Edge width indicates interaction strength.

In the case of SH-EP cells with a threshold of 0.012, the estimated networks included 478 edges and 99 nodes and had an average edge density of 4.83 (Figure 5). In these networks, three communities were identified by ModuLand [20], and each community node is shown as a different color. Eighty-eight percent of genes in the networks appeared in the leftmost community. Twenty-three genes had node degrees above 10, and their regulation structure is shown in Figure 6. Except for genes including *MSH6* (mutS homolog 6) and *RBCK1* (RanBP-type and C3HC4-type zinc finger containing 1), all hub genes came from the same community, including cyan node. The topmost gene *MSH6* encodes a member of the DNA mismatch repair MutS family, which helps in the recognition of mismatched nucleotides prior to their mismatch [23]. This gene showed negative association with *RBCK1*, whose gene product has a function of E3 ubiquitin-protein ligase. E3 ubiquitin-protein ligase accepts ubiquitin from specific E2 ubiquitin-conjugating enzymes and transfers it to its substrates [24]. At 24 h after MPP⁺ treatment, *MSH6* and *RBCK1* showed down-regulation (fold change = 0.47) and up-regulation (fold change = 2.0), respectively. The negative association of *MSH6* and *RBCK1* showed a good agreement with their regulation patterns. In addition, the down-regulation of *MSH6* may induce DNA damage and increase the number of misfolded proteins, which result in the up-regulation of ubiquitination-related genes, such as *RBCK1*. This indicates that MPP⁺ might induce the acceleration

of DNA damage and ER stress by misfolded proteins in SH-EP cells. Positive auto-regulation was observed at all hub genes except for *MTHFD2* (methylenetetrahydrofolate dehydrogenase [NADP⁺-dependent] 2) and *ZCCHC8* (zinc finger, CCHC domain containing 8). Positive auto-regulation may contribute to the continuous increase or decrease in gene expression patterns. The fold changes of zinc finger genes, such as *ZCCHC8*, *ZNF772* (zinc finger protein 772) and *ZNF26* (zinc finger protein 26), were high at 12 and 24 h after MPP⁺ treatment (Table S2).

This indicates that regulated or targeted genes by these zinc finger proteins might play a role in MPP⁺ toxicity. The hub gene *TRIB3* (tribbles pseudokinase 3), which is involved in DDIT3/CHOP-dependent cell death during ER stress, showed very high fold changes at 24 h after MPP⁺ treatment, whereas the expression of hub gene *NINJ2* (ninjurin 2), which may have a role in nerve regeneration after nerve injury, showed a time-dependent decrease. It is interesting to note that RNA genes, such as *RNU86* (U86 small nucleolar RNA), *EPB41L4A* (EPB41L4A antisense RNA 1), *SNHG1* (small nucleolar RNA gene 1), and *C7orf40* (small nucleolar RNA host gene 15), were observed in the hub gene networks, and most of their expression showed time-dependent increases. Two hub genes, including *CTH* (cystathionine gamma-lyase) and *CARS* (cysteinyl-tRNA synthetase), showed up-regulation from 9 h after MPP⁺ treatment (Table S2). The cells under oxidative stress can require high amounts of cysteine, because the synthesis of glutathione might depend on its availability, which may be the most important intracellular defense against oxidative stress. Thus, the increasing expression values of *CTH* and *CARS* in MPP⁺-treated SH-EP cells might indicate that MPP⁺-triggered oxidative stress might increase with time.

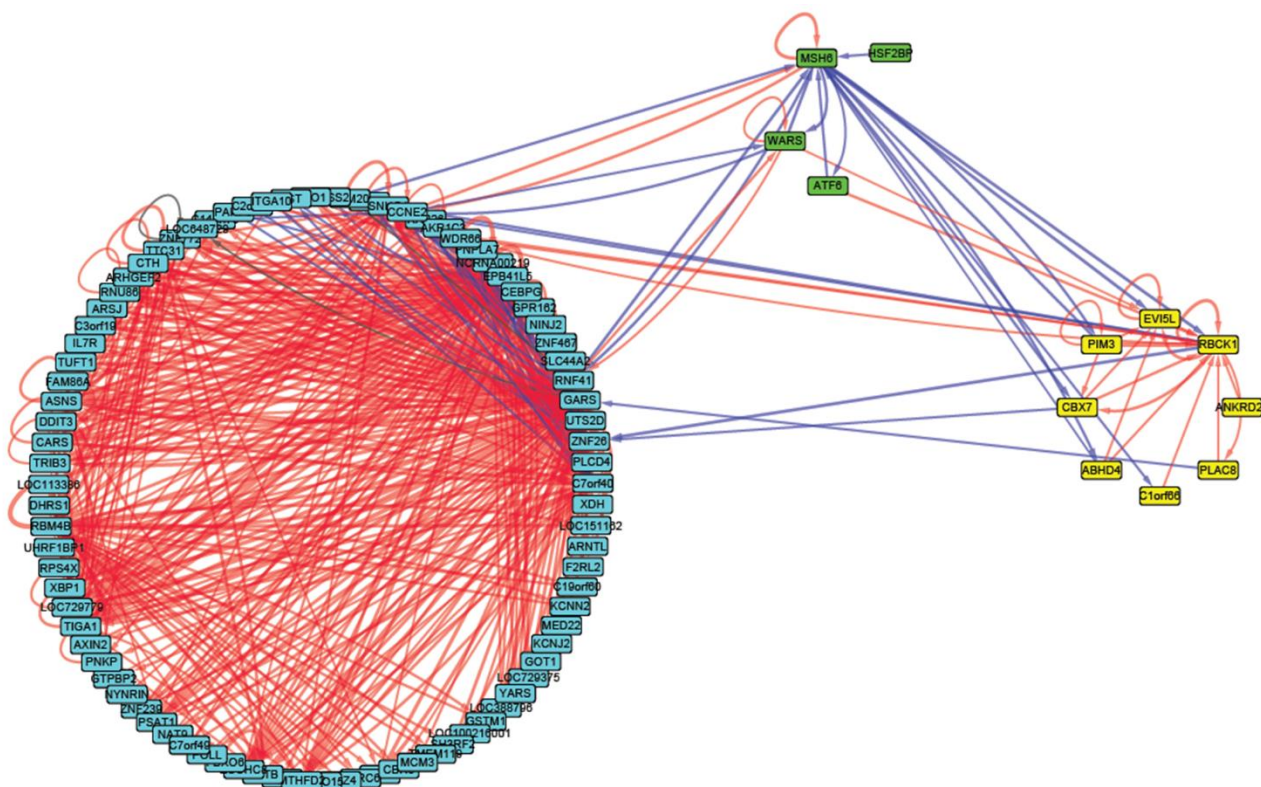


Figure 5. Estimated gene networks with a threshold of 0.012 for SH-EP cells. The positive and negative associations are represented by red and blue arrows, respectively. The networks consisted of three communities and each community was gathered with same color of node.

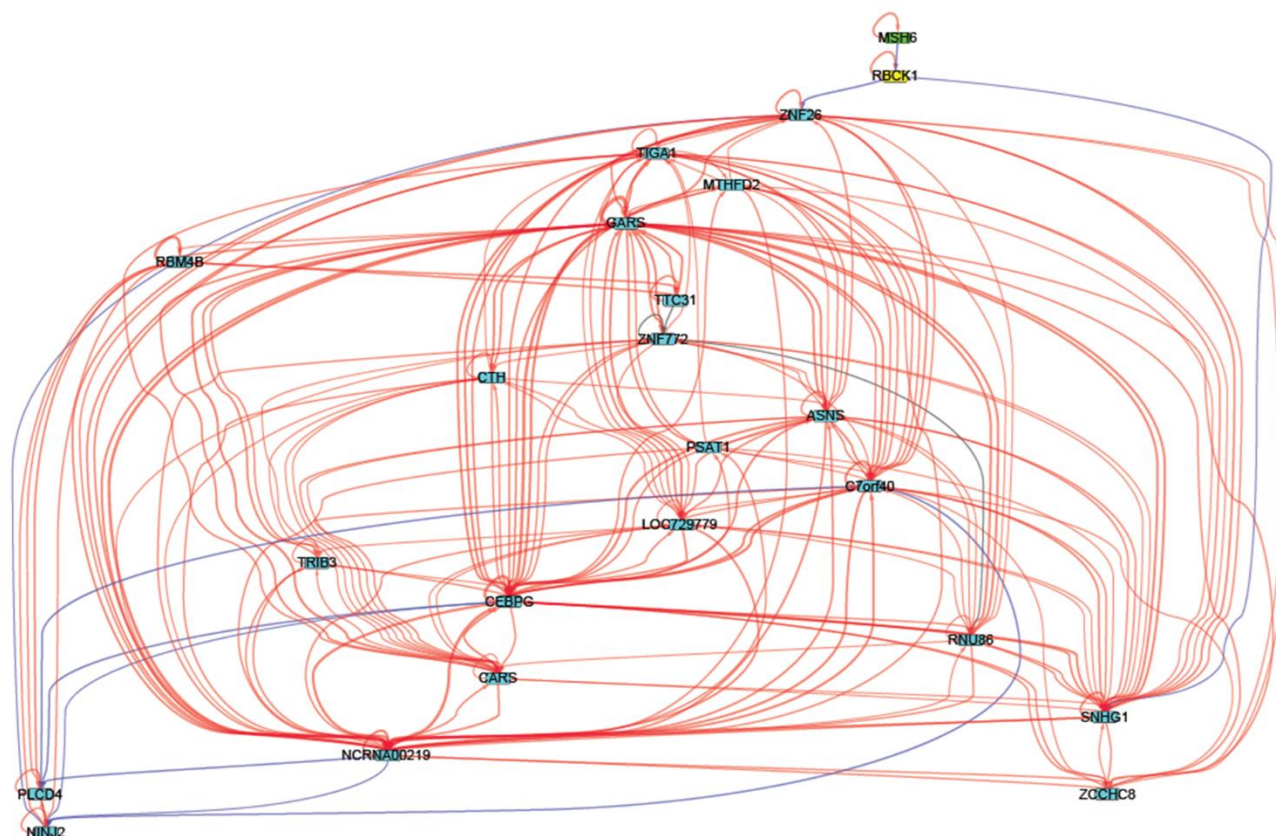


Figure 6. Sub-networks extracted from Figure 5 by selection of nodes, which have node degrees above 10. The positive and negative associations are represented by red and blue arrows, respectively. Edge width indicates interaction strength.

4. Conclusions

Growing evidence suggests that the mitochondrion-dependent programmed cell death (PCD) pathways may lead to different morphological types of cell death in the brain of PD patients [10]. This suggests that PCD pathways that are triggered by the inhibition of complex I might result in cell death via various downstream processes, such as mitochondrion-mediated caspase-dependent apoptosis or caspase-independent non-apoptotic cell death. The factors that affect various downstream processes of mitochondrial complex I inhibition are unknown. Therefore, various downstream processes of mitochondrial complex I inhibition should be considered as potential neuroprotective strategies for PD. Because the inhibition of mitochondrial complex I by MPP⁺ reproduces several PD-linked cellular alterations, such as increased production of ROS, oxidative damage to lipids, DNA, and proteins [25-27], MPP⁺-treated cells have been employed as a PD model. We compared MPP⁺ responses in two types of human neuroblastoma cells (SH-SY5Y and SH-EP), which were derived from the common cell line SK-N-SH, but their morphologies and biochemical properties are different. SH-SY5Y cells belong to the N-type which has neuroblast characteristics, such as neurotransmitter biosynthetic enzymatic activities and catecholamine uptake. In contrast, SH-EP cells are similar to immature glial cells (S-type), because they are not neuronal but do produce type I and III collagens [28].

SH-SY5Y and SH-EP cells shared only 14% of their own MPP⁺ response genes. GO analysis for these common MPP⁺ response genes showed significance in ER stress by misfolded proteins. This

indicates that ER stress by misfolded proteins might play a key role in MPP⁺-induced neuronal cell death. However, the mechanism that relates complex I inhibition to ER stress by misfolded proteins might be different, as 86% of their own MPP⁺ response genes displayed cell-type specificity. To identify groups of influential genes, i.e., gene modules, during MPP⁺-induced neuronal cell death, the SSM consisting of system and observation model was employed. Time-dependent expression values of MPP⁺ response genes were used for the estimation of SSM parameters, which provides a basis of module and gene interactions. Gene expression patterns within the same gene module were quite similar, which suggests the coordinate regulation of genes in the same module (Figure 1). As module genes have influential effects on the expression of other genes, their interaction structure might provide an insight into MPP⁺-induced neuronal cell death. Interactions in gene levels were estimated using parameters of the SSM, which were calculated during the module identification process. Gene networks for SH-SY5Y and SH-EP cells were constructed based on the gene-level interaction matrix. In the SH-SY5Y networks, a hub gene, *HIST1H2BK*, was severely down-regulated at 24 h after MPP⁺ treatment (Table S2). This indicates that the MPP⁺-mediated inhibition of mitochondrial complex I might affect nucleosome structure. Nucleosomes are consisting of four major classes of histones (H3, H4, H2A, and H2B) [29] and build the basic units of eukaryotic chromatin. Packaged DNA into chromatin also plays as a key regulator with transcriptions factors [30]. Two hub genes, *MSH6* and *RBCK1*, were down-regulated and up-regulated at 24 h after MPP⁺ treatment (Table S2) in the SH-EP networks, respectively.

This suggests that MPP⁺-mediated inhibition of mitochondrial complex I might induce ER stress by misfolded proteins, which might be produced via DNA mutation. The comparison of two networks indicates that the MPP⁺-mediated inhibition of mitochondrial complex I might induce neuronal cell death via various cellular downstream processes rather than a single determined process. Therefore, nucleosome structure defects and ER stress by misfolded proteins might be key downstream processes for MPP⁺ treated SH-SY5Y and SH-EP cells, respectively. This result might explain why postmortem PD patients exhibit variations in cell death types, such as mitochondrion-mediated caspase-dependent apoptosis and caspase-independent nonapoptotic cell death. In addition, hub genes in SH-SY5Y and SH-EP networks might be considered as potential targets for PD treatment or therapy.

Acknowledgments

This study was supported by the Basic Science Research Program through the National Research Foundation of Korea (NRF) funded by the Ministry of Education, Science and Technology (MEST) (No.2012R1A1A2005622), and was also supported by Dong Yang University in the year 2014.

Conflicts of Interest

The author declares no conflict of interest.

References

1. Dawson TM, Ko HS, Dawson VL (2010) Genetic animal models of Parkinson's disease. *Neuron* 66: 646-661.
2. Ribeiro RP, Moreira EL, Santos DB, et al. (2003) Probulcol affords neuroprotection in a 6-OHDA mouse model of Parkinson's disease. *Neurochem Res* 38: 660-668.

3. Lu C, Zhang J, Shi X, et al. (2014) Neuroprotective effects of tetramethylpyrazine against dopaminergic neuron injury in a rat model of Parkinson's disease induced by MPTP. *Int J Biol Sci* 10: 350-357.
4. Langston JW, Ballard P, Tetrud JW, et al. (1983) Parkinsonism in humans due to a product of meperidine- analog synthesis. *Science* 219: 979-980.
5. Dagda RK, Das Banerjee T, Janda E (2013) How Parkinsonian toxins dysregulate the autophagy machinery. *Int J Mol Sci* 14: 22163-22189.
6. Behl C, Davies JB, Lesley R, et al. (1994) Hydrogen peroxide mediates amyloid protein toxicity. *Cell* 77: 817-827.
7. Xiang W, Schlachetzki JC, Helling S, et al. (2013) Oxidative stress-induced posttranslational modifications of alpha-synuclein: Specific modification of alpha-synuclein by 4-hydroxy-2-nonenal increases dopaminergic toxicity. *Mol Cell Neurosci* 54: 71-83.
8. Zhou M, Xu S, Mi J, et al. (2013) Nuclear translocation of alpha-synuclein increases susceptibility of MES23.5 cells to oxidative stress. *Brain Res* 1500: 19-27.
9. Varcin M, Bentea E, Michotte Y, et al. (2012) Oxidative stress in genetic mouse models of Parkinson's disease. *Oxid Med Cell Longev* 2012: 624925.
10. Perier C, Bové J, Vila M (2012) Mitochondria and programmed cell death in Parkinson's disease: apoptosis and beyond. *Antioxid Redox Signal* 16: 883-895.
11. Chakraborty S, Bornhorst J, Nguyen TT, et al. (2013) Oxidative stress mechanisms underlying Parkinson's disease-associated neurodegeneration in *C. elegans*. *Int J Mol Sci* 14: 23103-23128.
12. Kim IS, Choi D.-K., Do J.H. (2013) Genome-wide temporal responses of human neuroblastoma SH-SY5Y cells MPP⁺ neurotoxicity. *BioChip J* 7: 247-257.
13. Do JH (2014) Neurotoxin-induced pathway perturbation in human neuroblastoma SH-EP cells. *Mol Cells* 37: 672-684.
14. Do JH, Kim IS, Lee JD, et al. (2011) Comparison of genomic profiles in human neuroblastic SH-SY5Y and substrate-adherent SH-EP cells using array comparative genomic hybridization. *BioChip J* 5: 165-174.
15. Hirose O, Yoshida R, Imoto S, et al. (2008) Statistical inference of transcriptional module-based gene networks from time course gene expression profiles by using state space models. *Bioinformatics* 24: 932-942.
16. Leek JT, Monsen E, Dabney AR, et al. (2006) EDGE: extraction and analysis of differential gene expression. *Bioinformatics* 22: 507-508.
17. Eden E, Navon R, Steinfeld I, et al. (2009) Gorilla: a tool for discovery and visualization of enriched GO terms in ranked gene list. *BMC Bioinformatics* 10: 48.
18. Yamaguchi R, Yoshida R, Imoto S, et al. (2007) Finding module-based gene networks with state-space models. *IEEE Signal Proc Mag* 24: 37-46.
19. Tamada Y, Yamaguchi R, Imoto S, et al. (2011) SiGN-SSM: open source parallel software for estimating gene networks with state space model. *Bioinformatics* 27: 1172-1173.
20. Kovács IA, Palotai R, Szalay MS, et al. (2010) Community landscapes: an integrative approach to determine overlapping network module hierarchy, identify key nodes and predict network dynamics. *PLoS One* 5: e12528.
21. Wang X, Dalkic E, Wu M, et al. (2008) Gene-module analysis: identification to networks and dynamics. *Curr Opin Biotechnol* 19: 482-491.

22. Pinho R, Garcia V, Irimia M, et al. (2014) Stability depends on positive autoregulation in Boolean gene regulatory networks. *PLoS Comput Biol* 10: e1003916.
23. Iaccarino I, Marra G, Palombo F, et al (1998) hMSH2 and hMSH6 play distinct roles in mismatch binding and contribute differently to the ATPase activity of hMutS α . *EMBO J* 17: 2677-2686.
24. Ardley HC, Robinson PA (2005) E3 ubiquitin ligases. *Essays Biochem.* 41: 15-30.
25. Wu DC, Jackson-Lewis V, Vila M, et al. (2002) Blockage of microglial activation is neuroprotective in the 1-methyl-4-phenyl-1, 2, 3, 6-tetrahydropyridine mouse model of Parkinson disease. *J Neurosci* 22: 1763-1771.
26. Perier C, Tieu K, Guégan C, et al. (2005) Complex I deficiency primes Bax-dependent neuronal apoptosis through mitochondrial oxidative damage. *Proc Natl Acad Sci USA* 102: 19126-19131.
27. Hoang T, Choi DK, Nagai M, et al. (2009) Neuronal NOS and cyclooxygenase-2 contribute to DNA damage in a mouse model of Parkinson disease. *Free Radic Biol Med* 47: 1049-1056.
28. Shinohara T, Nagashima K, Major EO (1997) Propagation of the human polyomavirus, JCV, in human neuroblastoma cell lines. *Virology* 228: 269-277.
29. Hondele M, Ladurner AG (2011) The chaperone-histone partnership: for the greater good of histone traffic and chromatin plasticity. *Curr Opin Struct Biol* 21: 698–708.
30. Smith KT, Workman JL (2012) Chromatin proteins: key responders to stress. *PLoS Biol* 10: e1001371.

Supplementary

Table S1. Module genes of SH-SY5Y and SH-EP cells, as estimated by the state space model.
Table S2. Fold changes of node genes shown in Figures 3 (networks of SH-SY5Y cells) and 5 (networks of SH-EP cells) at each time point after MPP⁺ treatment. Provided as separate files.



AIMS Press

© 2015 Jin Hwan Do, licensee AIMS Press. This is an open access article distributed under the terms of the Creative Commons Attribution License (<http://creativecommons.org/licenses/by/4.0>)